NASA TECHNICAL NOTE

NASA TN D-3258

EXPERIMENTAL EVALUATION OF VARIOUS NONMETALLIC ABLATIVE MATERIALS AS NOZZLE SECTIONS OF HYDROGEN-OXYGEN ROCKET ENGINE

by Reino J. Salmi, Alfred Wong, and Ralph J. Rollbuhler

Lewis Research Center

Cleveland, Ohio

NATIONAL AERONAUTICS AND SPACE ADMINISTRATION • WASHINGTON, D. C. • MARCH 1966

EXPERIMENTAL EVALUATION OF VARIOUS NONMETALLIC ABLATIVE

MATERIALS AS NOZZLE SECTIONS OF HYDROGEN-

OXYGEN ROCKET ENGINE

By Reino J. Salmi, Alfred Wong, and Ralph J. Rollbuhler

Lewis Research Center
Cleveland, Ohio

EXPERIMENTAL EVALUATION OF VARIOUS NONMETALLIC ABLATIVE MATERIALS AS

NOZZLE SECTIONS OF HYDROGEN-OXYGEN ROCKET ENGINE

by Reino J. Salmi, Alfred Wong, and R. James Rollbuhler

Lewis Research Center

SUMMARY

An investigation was conducted to evaluate 40 nonmetallic ablative materials as the nozzle section of a 150-pound-nominal-thrust, gaseous-hydrogen - liquid-oxygen rocket engine operating at an initial nominal chamber pressure of 100 pounds per square inch absolute, a throat diameter of 1.2 inches, and an oxidant-fuel ratio of approximately 6.7. These commercially available materials were either nonreinforced or reinforced with woven cloths such as silica, graphite, carbon, or asbestos and with phenolic or epoxy resins. The results, which were obtained with an engine operating with a c^* efficiency of approximately 93 percent and therefore not representative of a high-performance system, were used only for comparative purposes.

The results of this study are presented as a rating of materials based on nozzle throat erosion and weight loss. The best erosion resistance was obtained with silica-cloth-reinforced materials containing either polyamide-modified phenolic or phenolic with silica powder filler. No correlation between erosion rate and char depth was obtained. The combustion efficiency of the test engine, as would be expected, influenced the nozzle erosion rate.

INTRODUCTION

Ablatively cooled thrust chambers are being used in a number of liquid-propellant rocket applications (e.g., the Titan transtage engine and all modules of the Apollo spacecraft). Compared to the complexity of a regeneratively cooled rocket engine, the simplicity and potential reliability of an ablatively cooled engine are very attractive. Specific advantages of the ablative engine, which result from elimination of regenerative cooling passages, are lower propellant tank pressures in pressurized propellant systems and the elimination of cooling problems associated with deep throttling.

To be competitive with other types of rocket engines, an ablatively cooled engine must exhibit substained high performance during its operating life. However, the philosophy of ablative cooling (i.e., the absorption of heat by mass loss) is contrary to that for high rocket engine performance, which requires that the nozzle throat area remain relatively constant. The problem of preventing excessive erosion in the ablative engine throat is further aggravated by the fact that the throat region experiences the highest heat flux from

the high-temperature exhaust gases.

The ablative process, as described in reference 1, consists of various chemical reactions and heat-transfer processes. In a rocket nozzle throat these reactions and processes depend not only on the properties of the ablative material but also on the exhaust gas temperature, composition, and flow properties. The erosion rate of an ablative material in a rocket nozzle is, therefore, very difficult to predict analytically. The suitability of an ablative material for application as a rocket engine nozzle is best determined, therefore, from tests of the material under the conditions at which it is to be used.

Most of the ablative materials available are rated by the manufacturers on the basis of comparative tests made with high-temperature torch flames (e.g., refs. 2 and 3). Some evaluation studies of ablative materials fabricated as an integral part of a rocket system, usually as the nozzle component, are reported in references 4 and 5. Solid propellants have been utilized in some of these studies (ref. 5); however, because test conditions differ from those for liquid propellants, materials which apparently are adequate for one type of propellant may not be suitable for the other. Unfortunately, the limited results from reference 3 indicate that most of the materials had high erosion rates and would be inadequate for rocket engine nozzles and combusion chambers. A preliminary investigation was conducted, therefore, at the Lewis Research Center to evaluate some commercially available nonmetallic ablative materials under actual rocket firing conditions in order to screen the many candidates and identify those which appeared most promising for liquid-propellant rocket engine application.

Forty ablative materials were tested as the nozzle section of a gaseous-hydrogen - liquid-oxygen rocket engine operating at an initial chamber pressure of 100 pounds per square inch absolute, an oxidant-fuel ratio of about 6.7, and an initial throat diameter of 1.2 inches.

In the present investigation, no attempt was made to select the best material but only (1) to narrow the number of materials which would warrant further testing or development, (2) to determine some general trends among the material variables, and (3) to indicate correlations among the measured results.

The results of this study are presented primarily in the form of plots of throat erosion and nozzle weight loss against run time. Char depth and temperature measurements are also presented for some materials.

APPARATUS

Ablative Materials

The ablative materials tested in this preliminary screening program are listed in table I, which cites the vendor of each sample and gives a general description of the material composition. In some instances information was not available and this is indicated. The NASA code number assigned to each sample

2

is listed along with the vendor code number; however, the NASA number will be used to identify the samples hereinafter. A majority of the samples had a phenolic or epoxy novolac resin system or modifications thereof. Most of the samples were fabricated from a woven cloth or tape and were denoted as reinforced. A majority of these reinforcing materials were woven from high-purity silica fibers; others were made of carbon, graphite, or an asbestos. The remaining samples were a mixture of various constituents and were deemed nonreinforced. The fiber angles presented are measured relative to the nozzle centerline. A 90° orientation indicates that the fibers were normal to the centerline, and the acute angles indicate that the fiber ends at the nozzle surface were pointing downstream. The 1/2-by-1/2-inch material is a molded block of 1/2-inch squares of woven fibers which were randomly oriented, until molded, when the square pieces became oriented in parallel planes. Besides the variables mentioned previously, the fabrication techniques (e.g., curing cycles, consisting of varying temperatures, pressures, and times) differed, especially from vendor to vendor. No physical or chemical analyses were conducted on these samples, and the information listed in table I was obtained solely from the vendors.

Facility

The investigation was conducted in a small rocket test facility which was capable of supplying gaseous hydrogen and liquid oxygen at 140° R. Gaseous fluorine at ambient temperature was used for ignition. A schematic diagram of the propellant flow system is shown in figure 1.

Test Engines

The basic engine configuration used in this study is shown disassembled in figure 2. The injector, combustion chamber, and test nozzle, as shown in figure 3, were held together by pneumatic clamps. In most instances the nozzle sealed against the combustion chamber only from the pressure applied by the pneumatic clamps; however, other nozzles were slipped into a metal sleeve which was welded to the end of the standard chamber, and an O-ring around the outside of the nozzle helped to prevent gas leakage between the chamber and the nozzle (note O-ring groove on nozzle in fig. 4). Nozzles 49, 50, 51, 52, 53, and 55 were installed in this manner.

As will be discussed later, it became necessary to use a third method of nozzle attachment, shown in figure 5, with nozzles 32-2 and 32-3. In this fixture the nozzle was slipped into a metal sleeve, and a metal retainer was hand screwed into place at the upstream end of the nozzle. This attachment method prevented any axial pressure on the ablative nozzles. Gas leakage was prevented by the metal O-rings strategically placed at the chamber-retainer interface and at the retainer-nozzle surface, as indicated in figure 5.

Injector. - The engine employed a 45-element converging showerhead type of injector. The injector, shown in figure 6, was made up of concentric rings of hydrogen elements (33) and oxygen elements (12), which were positioned so that all propellant streams converged at a common point on the combustion chamber

3

centerline approximately 6 inches from the injector face.

Combustion chambers. - The combustion chamber was a nominally 6-inch-long, water-cooled, stainless-steel, cylindrical section with a 2.35-inch inside diameter. A 0.04-inch-thick coating of zirconia was placed on the inside surface to reduce the heat loss through the chamber walls. A 10-inch-long chamber similar to the 6-inch chamber was fabricated and was used in comparative tests with one nozzle material.

Ablative test nozzles. - As the specimens were received, they were machined into the standard inner configuration, shown in figure 7. The nozzles were 4 inches long and had a 2.31-inch inside entrance diameter, which converged to a nominally 1.2-inch-diameter tubular throat 1 inch long. For expediency, the external geometry of the nozzles was not standardized. The samples were used as received, and they were either 3.5-inch-diameter cylinders 4 inches long or 4-inch cubes. It was felt that, for the determination of erosion rates, the differences in external geometry would have only second-order effects. In the case of the reinforced materials, the samples were machined so that the fibers were either perpendicular to the nozzle centerline or directed downstream relative to the exhaust gas flow. The samples made from 1/2-inch squares of woven cloth were machined so that the parallel planes of the square pieces of cloth were normal to the nozzle centerline.

Instrumentation

The combustion chamber pressure was measured by strain-gage-type transducers. Metering orifices were used to measure both propellant flow rates. Additionally a turbine flowmeter measured the oxygen flow. Thrust was not measured. Twelve Chromel-Alumel thermocouples, four at each of three axial planes, 0.5, 1.0, and 2.0 inches from the exit plane, and located at varying depths were used to measure wall temperatures of most of the nozzles during each run. Figure 7 gives the nominal distance from the inner surface of each thermocouple. The two views in figure 7 are sections at 90° to each other. All pressure transducer and thermocouple outputs were continuously recorded on a multichannel, variable-speed oscillograph. Backup data were monitored on self-balancing potentiometer strip charts.

PROCEDURE

The instrumentation equipment was calibrated, and the assembled test engine was pressure checked before each run. The liquid-oxygen tank was pressurized by regulated helium gas, and the gaseous-hydrogen coil pressure was controlled by a pressure regulator in the line between the main hydrogen trailer and the hydrogen coil. The pressures were set to obtain the desired initial chamber pressure of 100 pounds per square inch absolute and oxidant-fuel ratio of 6.7. During the course of a run, the nozzle throat erosion reduced the chamber pressure and caused a variation in the oxidant-fuel ratio between about 5.0 and 7.0 since no oxidant-fuel-ratio controller was used. A sequence timer automatically activated the appropriate valves and data acquisition equipment and set the duration of the propellant line purges for each run.

In the early phase of the program, test nozzles were subjected to preset run durations, usually for progressively increasing time periods. For some of the longer firings or poorer materials, the chamber pressure decreased considerably. It was decided, therefore, to terminate a test when the chamber pressure, because of throat erosion, decayed to 90 pounds per square inch absolute or when the propellant supply became exhausted, whichever occurred first.

To obtain meaningful results from comparative tests of various ablative materials, it was necessary to maintain a uniform engine combustion efficiency. The test engine (i.e., injector) was periodically checked at the program test conditions to determine if its performance level was changing during the course of the investigation. This performance check was accomplished by substituting a metal heat-sink nozzle (fig. 8) for the ablative test nozzle and conducting short-duration tests at the specified test conditions.

The performance level of the test engine was based on characteristic exhaust velocity efficiency ηc^*, which is defined as

$$\eta c^* = \frac{c^*_{actual}}{c^*_{theoretical}} \times 100$$

and is indicative of the combustion efficiency of the engine. The c^*_{actual} for the test engine was calculated from the formula

$$c^*_{actual} = \frac{A_t P_c g}{W_t}$$

where P_c is the chamber pressure (lb/sq in. abs), A_t is the nozzle throat area (sq in.), g is the gravitational constant (ft/sec^2), and W_t is the total propellant weight flow rate (lb/sec). The theoretical c^* was obtained by the method of reference 6 modified to account for the gaseous hydrogen.

Before the initial test run and after each run the ablative test nozzles were X-rayed and weighed and the throat diameter was measured. Early in the investigation the throat diameter was determined by averaging four measurements taken by means of inside calipers, but as the throat eroded and became more eccentric, this technique obviously became less accurate; therefore, an optical comparator with a magnification of 10 was incorporated. The outline of the nozzle throat obtained by the comparator was planimetered, and an effective diameter was calculated from the resulting area. Test nozzles were axially bisected, and the char depth was measured after testing was completed, usually when the nozzle throat radius had increased by 0.13 inch. These measurements, along with other basic information, are listed in table II.

RESULTS AND DISCUSSION

Engine Performance

As pointed out in the previous discussion, the engine c^* efficiency was determined from periodic check runs. The converging showerhead injector provided a c^* efficiency of approximately 93 percent of the theoretical value,

as determined with a nominally 6-inch-long cylindrical combustion chamber and a contoured metal nozzle. The periodic tests indicated that this level of efficiency was maintained throughout the test program. A c^* efficiency of 93 percent is not representative of a high-performance liquid oxygen - hydrogen system, but the results are useful for the comparative evaluation of the ablative materials. A nominally 10-inch-long cylindrical combustion chamber used for a comparative test with one ablative material increased the c^* efficiency about 2 percent.

Throat Erosion

The rate of increase of the nozzle throat area with time was selected as the primary parameter for evaluating ablative nozzle materials. Not only is the rocket engine performance directly affected by the size of the nozzle throat, but the greatest heat flux is experienced in this region. Except for throat erosion, ablative engines appear adequate in all other aspects.

The bar graphs of figure 9 indicate the time for each nozzle to reach specific increases in the average throat radius, 0.03, 0.056, and 0.113 inch, which correspond to area increases of 10, 20, and 40 percent, respectively. An ablative sample that is more erosion resistant than another will take a longer time to reach a specific radius increase. The materials in figure 9 are listed according to the time required to reach a 0.056-inch radius increase. Nozzle 67, which was made of silica cloth reinforcement material and a phenolic resin binder with silica powder additive (table I), required about 665 seconds of accumulated running time to reach a 0.056-inch radius increase; this was the longest time measured. In general, the silica-cloth-reinforced materials having either polyamide-modified phenolic or phenolic with silica powder filler binders exhibited higher erosion resistance than the other materials tested. There were insufficient data to determine any effects of reinforcing-material orientation. Photographs of a typical test nozzle before and after testing are presented in figure 10.

Nozzle Weight Loss

Another measure of the ablative material erosion rate is the variation of the nozzle weight loss with time. It is perhaps less meaningful in connection with the rocket engine because the relation between the weight loss and the nozzle throat area is not clearly defined. Also, in this case, the densities of the various ablative materials were not determined. The times for the nozzles to lose 25, 75, and 125 grams of weight are shown in figure 11. The materials are listed in the order of increasing time for 75-gram weight loss. These data again indicate the superiority of the silica-cloth-reinforced phenolic and the phenolic-modified materials for the conditions of these tests.

In figure 12, the weight loss of some typical test samples is shown as a function of the throat radius increase. The samples exhibited varying initial

rates of weight loss which were much greater than the steady state rates. In some cases, the throat radius decreased during the initial weight loss. Erosion of the tubular throat begins at the throat entrance, and the flow of the ablating material protects the downstream sections. This flow of the material, along with the initial thermal swelling of the sample, accounts for the high initial weight loss with little or even negative increases in throat radius.

Char Depth

In the description of the ablative process for a reinforced material (ref. 1), a steady-state condition was described wherein the char depth remained constant. Figure 13, which shows the char depth as a function of accumulated run time, indicates that for several cases an essentially steady-state condition was achieved. To correlate the erosion resistance with char depth, two theories based on the ablation model can be considered:

(1) For the same resin binder, and for equal temperature and strength properties for the char layer, the char depth will be directly related to its thermal conductivity; for example, nozzles 58 and 59 with graphite reinforcement, which has high conductivity, exhibit relatively deep char layers.

(2) If the various chars have equal conductivity, the char depth is proportional to mechanical strength or erosion resistance at elevated temperatures.

Hence, for a given binder, the char depth depends on conductivity and erosion resistance at elevated temperature. Also, the char depth will depend not only on the material properties of the reinforcement and resin, but also on their reaction with each other, fiber orientation relative to the surface, size of strands, relative densities, etc. Hence, a direct correlation between char depth and erosion resistance for a variety of materials would not be expected. The data of figure 14, which shows the maximum char depth of each material listed in order of increasing material erosion resistance (from fig. 9), indicate little or no correlation between char depth and erosion resistance.

Temperature

Typical temperature histories are given in figure 15 as a series of curves of nozzle temperature plotted against run time for nozzles 30 and 59. The measuring thermocouple (10) was initially approximately 0.175 inch from the inner surface and on an axial plane 0.5 inch from the nozzle exit plane (see fig. 7(b)). By noting that no decrease in chamber pressure occurred during the first 30 seconds of the first run for both nozzles, the lower conductivity of silica cloth (1 to 3 (Btu)(in.)/(sq ft)(hr)($^\circ$F)) compared to graphite cloth (5 to 6 (Btu)(in.)/(sq ft)(hr)($^\circ$F)) is confirmed since in 30 seconds the temperature of nozzle 30 was 300° F while nozzle 59 was at 1000° F. The greater shift to the left of curves for nozzle 59 for succeeding runs is indicative of a higher erosion rate for nozzle 59 than for nozzle 30.

Effects of Testing Techniques

The effect of nozzle run duration on the throat erosion rate was determined by testing two nozzles made of the same material. One nozzle (30) was run for short fixed durations and the other nozzle (30-2) was tested until the chamber pressure dropped to 90 pounds per square inch absolute. The nozzles differed only in that nozzle 30 was a 3.5-inch-outside-diameter cylinder whereas nozzle 30-2 was a nominally 4.0-inch cube. As shown in figure 16, the erosion rates of the two nozzles appeared similar up to an accumulated run time of 480 seconds, at which time the erosion rate of nozzle 30 drastically increased. Because of the differences in the external geometry of the two nozzles, the conclusions to be drawn are not clear-cut. However, it is believed that the effects of run duration or test technique were small and that the sudden rate increase for nozzle 30 was due to its smaller outside diameter. Examinations of the bisected nozzles showed that for nozzle 30 the char depth toward the nozzle entrance region approached the nozzle outer wall and, therefore, resin depletion in this region resulted in higher erosion rates at the throat. The temperature data also indicated higher material temperatures at the onset of the increased erosion rate of nozzle 30, which indicates loss of ablative cooling effects.

Testing Variables

Toward the later stages of the program, nozzle 32 was noticeably compressed axially by the pneumatic clamps. Consequently, the erosion rate was distorted because the ablative material was being squeezed into the throat region. To determine the effect of axial compression on the erosion rate, an identical sample of nozzle 32 material, designated as nozzle 32-3, was tested in the same facility but in the noncompressive fixture shown in figure 5. Figure 17 shows the difference in the effective throat erosion rate between the two samples. As expected, the compressed nozzle showed a lower effective nozzle radius increase, although the material weight loss (from table II) was 174 percent greater at the end of 567 seconds of accumulated run time.

To determine the effects of increased exhaust gas temperature on the erosion rate, another nozzle, denoted as 32-2 and identical to 32-3, was tested in the noncompressing holding fixture but attached to a longer combustion chamber (characteristic length $L^* = 44$, length $L = 10$ in. compared to $L^* = 30$, $L = 6.3$ in.). The nozzle throat radius increase is shown as a function of accumulated run time for the two nozzles in figure 18. As would be expected, the higher temperatures resulting from the more complete combustion (about 2-percent increase in c^* efficiency) in the longer chamber significantly increased the nozzle erosion rate.

SUMMARY OF RESULTS

A preliminary screening investigation of ablative materials as the nozzle section of a liquid-oxygen - gaseous-hydrogen rocket engine was conducted to determine some of the better nonmetallic ablative materials presently available for rocket thrust-chamber and nozzle applications. Because the results were ob-

tained with an engine operating at approximately 93 percent c^* efficiency and therefore are not representative of a high-performance liquid oxygen - hydrogen system, they are used only on a comparative basis and are summarized as follows:

1. Of the materials tested, those using silica-cloth reinforcement with a polyamide-modified phenolic resin or a silica-powder-modified phenolic resin exhibited the highest erosion resistance.

2. Nonreinforced materials, in general, exhibited poor erosion resistance.

3. Of the reinforcing materials only silica cloth exhibited relatively good erosion resistance.

4. No correlation was obtained between erosion resistance and char depth.

5. The effects of reinforcement orientation were not apparent.

6. As would be expected, combustion efficiency had a noticeable effect on the nozzle erosion rate.

Lewis Research Center,
    National Aeronautics and Space Administration,
        Cleveland, Ohio, September 17, 1965.

REFERENCES

1. Glaser, P. E., ed.: Aerodynamically Heated Structures. Prentice-Hall, Inc., 1962.

2. Buhler, R. D.; Christensen, Daphne; and Grindle, Shirley: Effects of Hyperthermal Conditions on Plastic Ablation Materials. Rept. No. ASD TR 61-304, Plasmadyne Corp., Oct. 1961.

3. Rashis, Bernard; and Walton, Thomas E., Jr.: An Experimental Investigation of Ablating Materials at Low and High Enthalpy Potentials. NASA TM X-263, 1960.

4. Schwartz, Herbert S.: Comparative Erosion Resistance of Plastic Materials in a Supersonic Rocket Exhaust and Subsonic Air Arc Plasma. Rept. No. TR 60-649, WADD, Sept. 1960.

5. Signorelli, Robert A.; and Johnston, James R.: Erosion Resistance and Failure Mechanisms of Several Nozzle Materials in a Small Solid-Propellant Rocket Engine. NASA TN D-1658, 1963.

6. Gordon, Sanford; and McBride, Bonnie J.: Theoretical Performance of Liquid Hydrogen with Liquid Oxygen as a Rocket Propellant. NASA MEMO 5-21-59E, 1959.

TABLE I. – PHYSICAL PROPERTIES OF ABLATIVE MATERIALS

Nozzle	Supplier	Supplier code number	Resin	Resin content, weight percent	Additives	Additive content, weight percent	Reinforcement material	Reinforcement form	Reinforcement content, weight percent	Fiber orientation with respect to nozzle centerline
16	AVCO	X2001	Epoxy novalac	30	None	--	Silica	Cloth	70	90°
17	HITCO	None available	Phenolic	30	None	--	Silica	Tape	70	15°
18	General Electric	3AS60	Epoxy novalac	40	Silica powder	60	None	-------	--	---
19	General Electric	3AR	Epoxy novalac	50	None	--	Silica	Cloth	50	90°
20	General Electric	X7R	Epoxy novalac	45	Buna N	5	Silica	Cloth	50	90°
22	General Electric	X3AC	Epoxy novalac	60	None	--	Carbon	Cloth	40	90°
23	General Electric	X3AOWR	Epoxy novalac	60	None	--	Silica	Cloth	40	90°
26	HITCO	None available	Phenolic	27	Buna N	3	Zirconia	Fibers	27	Random
28	Fiberite	MXS 19	Polyamide-phenolic	32	None	--	Silica	Cloth	68	90°
29	Fiberite	MXS 25	Polyamide-phenolic	32	Silica powder	8	Silica	Cloth	60	90°
30	Fiberite	MXS 75	Phenolic	31	Silica powder	8	Silica	Cloth	61	90°
30-2	Fiberite	MXS 75	Phenolic	31	Silica powder	8	Silica	Cloth	61	90°
32	Haveg	PL IV-1	Phenolic	30	Ceramic frit	6	Silica	1/2-in. squares	64	Random
32-2	Haveg	PL IV-1	Phenolic	30	Ceramic frit	6	Silica	1/2-in. squares	64	Random
32-3	Haveg	PL IV-1	Phenolic	30	Ceramic frit	6	Silica	1/2-in. squares	64	Random
34	Johns Manville	TX	Acrylic	45	None	--	Magnesia	Fibers	55	90°
35	Johns Manville	None available	Acrylic	52	None	--	Asbestos and graphite	Cloth	68	90°
36	Johns Manville	ARP 40	Phenolic	40	None	--	Asbestos	Fibers	60	90°
37	HITCO	S/N 401901	Phenolic	30	None	--	Silica	Cloth	70	Rosette pattern
38	Aerojet	None available	Phenyl silane	--	Buna N	--	Silica	Cordage tape	55	60°
39	Fiberite	MXR 42	Phenolic	27	Buna N	3	Magnesia	Fibers	60	90°
40	Raybestos Mannattan	150 RPD	Phenolic	40	None	--	Asbestos	Particles	60	Random
41	Raybestos Mannattan	41 RPD	Phenolic	27	None	--	Asbestos	Cloth	73	90°
42	Fiberite	MX 2625	Phenolic	25	Silica powder	11	Silica	1/2-in. squares	64	Random
43	Fiberite	MX 2646	Polyamide-phenolic	20	None	--	Silica	1/2-in. squares	80	Random
44	General Electric	223-10Q	Epoxy novalac	50	Silica powder	40	Silica	Fibers	10	Random
45	General Electric	227-10Q	Epoxy novalac	50	Silica powder	40	Silica	Fibers	10	Random
46	General Electric	227-15Q	Epoxy novalac	85	None	--	Silica	Fibers	15	Random
47	Fiberite	MX 2641	Phenolic	30	None	--	Silica	Cloth	70	90°
48	HITCO	C-155484	Phenolic	27	Chromium salts and Buna N	3	Silica	Cloth	70	90°
49	U.S. Rubber	3013	Phenolic	--	Boric Acid	--	None	-------	--	---
50	U.S. Rubber	3016	Styrene	50	None	50	Asbestos	-------	--	---
51	U.S. Rubber	3800	Buna N	50	None	50	Asbestos and silica	-------	--	---
52	Hughes Tool	32	Phenolic	35	Molybdenum boride powder	20	Silica	Cloth	45	90°
53	Hughes Tool	37	2,2-bis propane pheno-formaldehyde	35	None	--	Silica	Cloth	65	90°
55	U.S. Polyomeric	FM 5131	Phenolic	30	Pearlite	3	Silica	Cloth	67	60°
58	Fiberite	MXG 90	Phenolic	--	Refractory powder	--	Graphite	Cloth	--	90°
59	Fiberite	MX 4551	Phenolic	--	Silica powder	--	Graphite	Cloth	--	90°
64	Cincinnati Test Lab.	None available	Phenolic	45	None	--	Nylon	Cloth	55	90°
65	Cincinnati Test Lab.	None available	Phenolic	28	None	--	Silica	Cloth	72	90°
66	CORDO	R84-ACX	Phenolic	--	Silica powder	--	Silica	Cloth	75	90°
67	Haveg	MX 2600	Phenolic	31	Silica powder	8	Silica	Cloth	61	90°

TABLE II. - SUMMARY OF TEST RESULTS

Nozzle	Run duration, sec	Accumulated run time, sec	Chamber-pressure range, $P_{c,max}/P_{c,min}$, lb/sq in. abs	Oxidant-fuel ratio	Nozzle throat radius after run, in.	Throat radius growth rate, mils/sec	Nozzle weight after run, g	Accumulated weight loss, g	Maximum throat char depth, in.	
									Samples X-rayed after run	Bisected samples
16	0	0	-------	----	0.601	----	1784	---	----	-----
	29	29	96/90	6.41	.644	1.48	1752	32	0.33	-----
	40	69	93/87	6.15	.688	1.10	1733	51	.43	-----
	49	118	87/81	6.15	.712	.49	1707	77	.47	-----
	59	177	87/80	6.41	.776	1.31	1688	96	.49	0.48
17	0	0	-------	----	0.600	----	2234	---	----	-----
	30	30	105/106	6.64	.577	----	2212	22	0.15	-----
	40	70	105/98	7.55	.571	----	2192	42	.23	-----
	62	132	97/90	6.58	.625	0.87	2169	65	.26	-----
	80	212	90/87	6.20	.635	.13	2164	128	.32	-----
	100	312	108/89	6.25	.710	.75	2129	163	.28	-----
	101	413	105/54	7.07	1.010	2.97	1952	282	.24	0.17
18	0	0	-------	----	0.600	----	2354	---	----	-----
	30	30	110/112	6.47	.576	----	2317	37	0.21	-----
	40	70	105/97	7.93	.573	----	2279	75	.29	-----
	60	130	109/101	----	.663	1.50	2227	137	.48	-----
	80	210	97/80	6.00	.747	1.05	2132	229	.39	-----
	93	303	89/48	7.27	1.058	3.34	1817	537	----	-----
19	0	0	-------	----	0.600	----	1087	---	----	-----
	30	30	94/90	6.58	.622	0.73	1033	54	0.22	-----
	29	59	108/106	6.25	.634	.41	1005	82	.33	-----
	40	99	97/95	6.10	.663	.73	982	105	.40	-----
	60	159	103/95	5.71	.720	.95	949	138	.45	-----
	60	219	100/95	5.80	.765	.75	923	164	.50	-----
	59	278	85/82	6.15	.781	.27	909	178	.54	-----
20	0	0	-------	----	0.597	----	1059	---	----	-----
	30	30	108/107	6.30	.597	0.00	1012	47	0.23	-----
	40	70	103/98	6.20	.620	.58	988	71	.32	-----
	50	120	110/99	6.20	.657	.74	953	106	.34	-----
	60	180	100/90	5.85	.726	1.15	918	141	.39	-----
	60	240	92/89	5.62	.764	.63	892	167	.49	0.45
22	0	0	-------	----	0.600	----	952	---	----	-----
	29	29	100/96	5.67	.643	1.48	882	70	0.27	-----
	40	69	92/69	6.14	.849	5.15	802	150	.35	0.33
23	0	0	-------	----	0.598	----	1182	---	----	-----
	30	30	101/100	5.67	.595	----	1135	47	0.23	-----
	40	70	103/91	6.76	.640	1.13	1099	83	.37	-----
	59	129	96/82	6.69	.730	1.53	1052	130	.43	-----
	60	189	95/85	6.97	.803	1.22	1009	173	.48	0.48
26	0	0	-------	----	0.592	----	3153	---	----	-----
	31	31	103/96	6.35	.622	0.97	3110	43	----	-----
	39	70	95/73	7.00	.773	1.31	2977	176	0.07	0.175
28	0	0	-------	----	0.598	----	1154	---	----	-----
	30	30	89/89	6.25	.585	----	1124	30	0.19	-----
	39	69	102/101	6.36	.588	0.08	1109	45	.30	-----
	50	119	102/99	6.58	.605	.34	1091	63	.36	-----
	59	178	94/90	6.58	.614	.15	1080	74	.39	-----
	60	238	98/95	6.64	.637	.38	1070	84	.41	-----
	59	297	98/95	6.20	.631	----	1063	91	.44	-----
	60	357	92/88	6.41	.641	.17	1056	98	.43	-----
	70	427	96/91	6.00	.687	.66	1045	109	.42	-----
	79	506	101/93	5.90	.712	.32	1030	124	.47	-----
	81	587	90/85	5.45	.715	.04	1026	128	.47	-----
	91	678	96/85	6.30	.755	.44	1010	144	.52	-----
	100	778	89/51	6.20	1.006	2.51	876	278	.35	-----
29	0	0	-------	----	0.600	----	1141	---	----	-----
	30	30	98/97	6.52	.603	0.10	1115	26	0.18	-----
	40	70	98/97	6.64	.594	----	1103	38	.27	-----
	49	119	97/94	6.58	.599	.10	1085	56	.34	-----
	60	179	95/93	6.70	.606	.12	1073	68	.35	-----
	60	239	92/90	6.58	.622	.27	1061	80	.35	-----
	69	308	90/88	----	.637	.22	1052	89	.39	-----
	79	387	103/96	5.94	.660	.29	1039	102	.41	-----
	90	477	100/93	5.50	.692	.36	1033	108	.43	-----
	100	577	95/68	6.88	.840	1.48	977	164	.37	0.43
30	0	0	-------	----	0.601	----	1110	---	----	-----
	30	30	100/100	6.58	.600	----	1085	25	0.22	-----
	40	70	97/95	6.41	.591	----	1069	41	.30	-----
	50	120	94/93	6.36	.596	0.10	1057	53	.37	-----
	60	180	92/91	6.64	.604	.13	1045	65	.41	-----
	70	250	92/87	5.71	.623	.27	1034	76	.43	-----
	61	311	101/98	6.35	.657	.56	1027	83	.47	-----
	80	391	94/89	6.25	.679	.28	1016	94	.52	-----
	30	421	104/103	5.85	-----	----	----	---	----	-----
	60	481	104/102	6.00	.672	----	1008	102	.52	-----
	100	581	94/72	6.94	.852	1.80	941	169	.46	0.43

TABLE II. - Continued. SUMMARY OF TEST RESULTS

Nozzle	Run duration, sec	Accumulated run time, sec	Chamber-pressure range, P_c,max/P_c,min, lb/sq in. abs	Oxidant-fuel ratio	Nozzle throat radius after run, in.	Throat radius growth rate, mils/sec	Nozzle weight after run, g	Accumulated weight loss, g	Maximum throat char depth, in. Samples X-rayed after run	Bisected samples
32	0	0	-------	----	0.597	----	1400	---	----	------
	293	293	104/100	6.41	.583	----	1288	112	0.36	------
	274	567	110/91	----	.631	0.18	1235	165	.34	------
	73	640	95/88	6.75	.656	.34	1227	173	.36	------
	91	731	99/88	6.04	.695	.43	1211	189	.32	------
	81	812	90/85	6.20	.715	.25	1213	191	.28	0.60
32-2	0	0	-------	----	0.605	----	----	---	----	------
	113	113	86/74	6.41	.645	0.35	1129	---	----	------
	60	173	83/74	6.88	.685	.67	N.A.	---	----	------
	48	221	84/75	6.52	.731	.96	1100	---	----	------
	33	254	80/75	6.76	.765	1.03	1085	---	----	------
32-3	0	0	-------	----	0.600	----	1208	---	----	------
	92	92	84/83	6.94	.597	----	1167	41	----	------
	259	351	87/75	7.48	.646	0.18	1113	95	----	------
	118	469	88/75	6.64	.679	.28	1101	107	----	------
	99	568	84/67	6.82	.726	.47	1113	95	----	------
	27	595	78/74	6.76	.754	1.04	1081	127	----	------
34	0	0	-------	----	0.599	----	2012	---	----	------
	30	30	100/99	6.58	.595	----	1979	33	0.08	------
	40	70	84/83	4.72	.605	0.25	1961	51	.15	------
	60	130	111/92	6.58	.684	1.32	1917	95	.17	------
	71	201	102/68	6.52	.870	2.62	1810	202	.12	0.06
35	0	0	-------	----	0.599	----	981	---	----	------
	31	31	100/94	6.76	.678	2.54	904	77	0.40	0.40
36	0	0	-------	----	0.601	----	1132	---	----	------
	30	30	100/84	6.76	.679	2.60	1058	74	0.14	------
	41	71	89/62	6.70	.862	4.46	975	217	.09	0.07
37	0	0	-------	----	0.602	----	1137	---	----	------
	30	30	105/104	6.47	.601	----	1112	25	0.18	------
	40	70	95/92	6.09	.616	0.38	1099	38	.25	------
	60	130	99/90	6.41	.638	.37	1074	63	.34	------
	81	211	101/91	6.04	.706	.84	1049	88	.32	------
	101	312	91/60	6.04	.880	1.72	978	159	.23	0.34
38	0	0	-------	----	0.595	----	1023	---	----	------
	133	133	111/88	6.58	.630	0.26	878	145	0.43	------
	30	163	108/78	8.35	.760	4.33	660	363	.27	0.23
39	0	0	-------	----	0.597	----	1164	---	----	------
	31	31	103/162	6.15	.629	1.03	1127	37	0.11	------
	40	71	105/98	5.85	.694	1.63	1080	84	.16	------
	51	122	97/76	5.94	.947	4.96	1014	150	.20	0.08
40	0	0	-------	----	0.600	----	1145	---	----	------
	31	31	95/87	6.19	.650	1.61	1110	35	0.10	------
	40	71	103/72	6.09	.803	3.83	1037	108	.17	0.08
41	0	0	-------	----	0.602	----	1206	---	----	------
	31	31	103/81	6.81	.691	2.87	1147	59	0.12	------
	41	72	101/65	6.88	.936	5.98	1005	201	.11	0.04
42	0	0	-------	----	0.600	----	1157	---	----	------
	30	30	104/102	6.30	.601	0.03	1137	20	0.18	------
	40	70	105/104	6.47	.605	.10	1129	28	.25	------
	60	130	100/98	6.58	.615	.17	1113	44	.32	------
	80	210	98/89	6.76	.650	.44	1095	62	.35	------
	100	310	94/82	6.41	.685	.35	1067	90	.41	------
	59	369	94/91	6.52	.707	.37	1059	98	.42	------
	106	475	95/63	6.05	.880	1.63	967	190	.34	0.28
43	0	0	-------	----	0.601	----	1163	---	----	------
	30	30	103/101	6.47	.596	----	1144	19	0.18	------
	40	70	102/101	6.64	.592	----	1136	27	.25	------
	60	130	102/97	6.70	.627	0.58	1117	46	.37	------
	80	210	101/96	6.41	.636	.11	1100	63	.39	------
	100	310	100/94	6.58	.647	.11	1077	86	.39	------
	120	430	106/54	6.25	.915	2.23·	945	218	.34	0.32
44	0	0	-------	----	0.602	----	774	---	----	------
	31	31	108/99	6.64	.647	1.45	725	49	0.21	------
	41	72	98/69	6.58	.775	3.12	657	117	.15	0.12
45	0	0	-------	----	0.601	----	757	---	----	------
	30	30	105/104	6.36	.585	----	714	43	0.19	------
	40	70	103/96	6.70	.635	1.25	675	82	.27	------
	60	130	76/65	3.85	.700	1.08	628	129	.37	0.20
46	0	0	-------	----	0.598	----	591	---	----	------
	30	30	105/100	6.52	.600	0.07	544	47	0.16	------
	40	70	95/67	6.76	.760	4.00	485	106	.18	0.15

TABLE II. - Concluded. SUMMARY OF TEST RESULTS

Nozzle	Run duration, sec	Accumulated run time, sec	Chamber-pressure range, P_c,max/P_c,min, lb/sq in. abs	Oxidant-fuel ratio	Nozzle throat radius after run, in.	Throat radius growth rate, mils/sec	Nozzle weight after run, g	Accumulated weight loss, g	Maximum throat char depth, in.	
									Samples X-rayed after run	Bisected samples
47	0	0	-------	----	0.600	----	1925	---	----	-----
	29	29	99/101	6.15	.590	----	1907	18	0.18	-----
	40	69	102/101	6.52	.605	0.38	1895	30	.25	-----
	59	128	98/91	6.70	.650	.76	1874	51	.31	-----
	80	208	95/84	6.64	.700	.63	1850	75	.34	-----
	18	226	101/98	6.25	.730	1.67	1851	---	.35	-----
	100	326	95/82	6.09	.744	.14	1829	96	.40	-----
	106	432	90/53	6.58	.950	1.94	1727	198	.44	0.41
48	0	0	-------	----	0.605	----	1184	---	----	-----
	31	31	104/103	6.76	.596	----	1154	30	0.22	-----
	40	71	100/96	6.58	.600	0.10	1138	46	.29	-----
	60	131	96/89	6.52	.622	.37	1120	64	.38	-----
	80	211	101/92	6.64	.655	.41	1098	86	.30	-----
	100	311	107/85	6.04	.715	.60	1062	122	.53	-----
	120	431	96/60	6.52	.894	1.49	983	201	.44	0.41
49	0	0	-------	----	0.596	-----	----	---	----	-----
	2	2	93/89	7.00	-----	-----	610	---	----	-----
	26	28	90/38	7.20	1.160	20.14	350	260	----	-----
50	0	0	-------	----	0.600	-----	641	---	----	-----
	4	4	92/78	6.82	.699	24.75	611	30	----	-----
51	0	0	-------	----	0.600	-----	589	---	----	-----
	30	30	102/65	6.52	.911	10.37	507	82	----	-----
52	0	0	-------	----	0.600	----	893	---	----	-----
	91	91	103/89	6.47	.635	0.38	830	63	----	-----
	39	130	93/89	6.37	.647	.31	818	75	----	-----
	28	158	94/87	6.25	.692	1.61	805	88	----	0.27
53	0	0	-------	----	0.599	----	773	---	----	-----
	106	106	103/90	5.54	.608	0.08	693	80	0.20	-----
	240	346	109/91		.663	.23	616	157	.58	0.50
55	0	0	-------	----	0.599	----	817	---	----	-----
	280	280	101/98	6.35	.592	----	730	87	0.51	-----
	124	404	99/105	6.52	.631	0.31	694	123	.55	-----
	233	637	102/95	6.64	.660	.12	664	153	.47	0.50
58	0	0	-------	----	0.598	----	1961	---	----	-----
	91	91	101/89	5.85	.628	0.33	1826	135	0.65	-----
	27	118	95/	4.99	.651	.85	1817	144	.65	-----
	34	152	98/90	6.15	.700	1.44	1792	169	.40	0.62
59	0	0	-------	----	0.600	----	1964	---	----	-----
	128	128	98/88	5.85	.621	0.16	1800	164	0.63	-----
	40	168	97/89	5.06	.678	1.42	1785	179	.63	-----
	42	210	98/90	5.54	.722	1.05	1760	204	----	0.65
64	0	0	-------	----	0.600	----	1439	---	----	-----
	17	17	100/71	5.80	.733	7.82	1377	62	----	-----
	32	49	86/54	4.62	.952	6.84	1273	166	0.06	-----
65	0	0	-------	----	0.596	----	1821	---	----	-----
	168	168	101/101	6.09	.579	----	1760	61	0.55	-----
	4	172	96/91	7.78	-----	----	----	---	----	-----
	80	252	100/91	6.82	.625	0.55	----	---	.30	-----
	116	368	100/89	6.52	.668	.37	1730	91	.46	-----
	84	452	-------	----	.676	.10	----	---	.43	-----
	78	530	98/89	6.69	.706	.38	----	---	.45	-----
	30	560	91/88	6.00	.731	.83	----	---	.40	0.40
66	0	0	-------	----	0.598	----	1845	---	----	-----
	270	270	100/92	6.24	.609	0.04	1740	105	0.72	-----
	162	432	103/90	6.41	.653	.27	1742	123	.58	-----
	119	551	96/89	6.64	.685	.27	1707	138	.63	-----
	20	571	100/99	5.13	.690	.25	1615	230	N.A.	0.61
67	0	0	-------	----	0.596	----	1762	---	----	-----
	297	297	102/102	6.30	.575	----	1704	58	0.51	-----
	13	310	106/106	6.41	.575	0.	1707	55	.55	-----
	274	584	107/90	7.07	.626	.19	1649	113	.60	-----
	82	666	92/	6.52	.652	.32	----	---	.60	-----
	239	905	100/88	6.58	.698	.19	----	---	.57	-----
	38	933	92/90	6.88	.729	1.11	----	---	.54	-----
	61	1004	94/90	6.10	.745	.26	----	---	.55	0.62

Helium pressurizing gas

Hydrogen gas

Oxidant system vent

Oxidant tank submerged in liquid-nitrogen bath

Pressure regulators

Oxygen load line

Fuel system vent

Orifices

Turbine flowmeter

Fire valves

Oxidant purge

Fluorine ignition gas

Coolant water

Fuel line coiled and submerged in liquid-nitrogen bath

Fuel purge

Ablative nozzle being tested

CD-8223
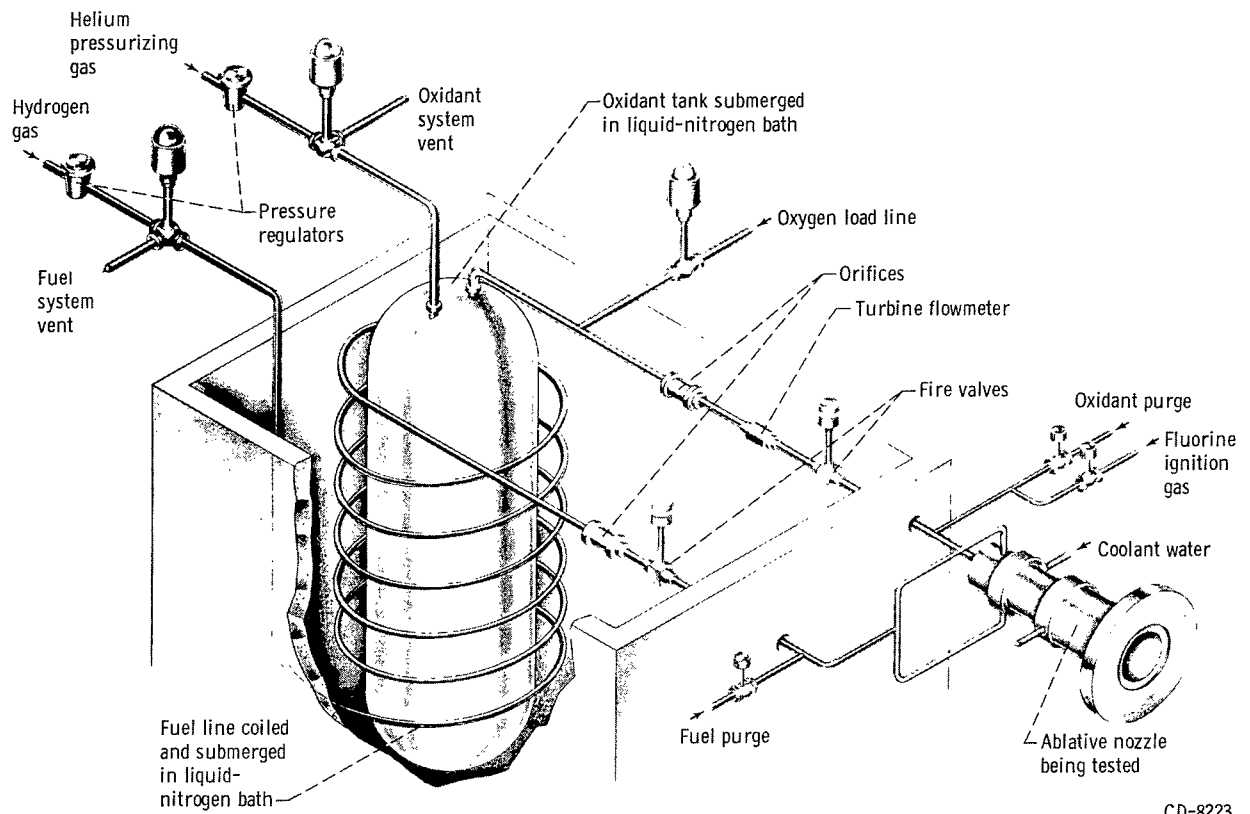
Figure 1. – Schematic view of test equipment.

Injector

Water-cooled combustion chamber

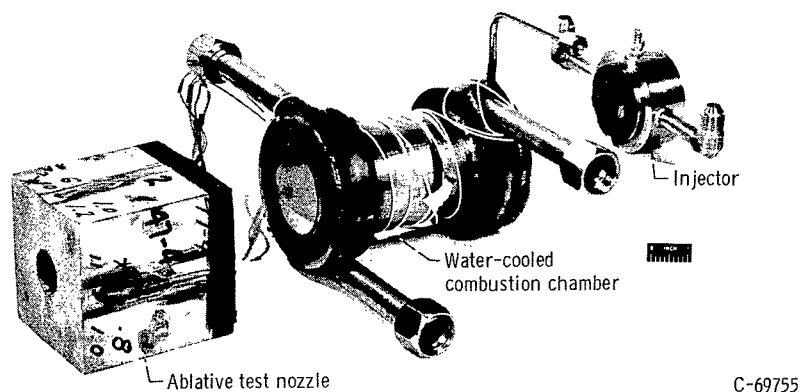Ablative test nozzle

C-69755

Figure 2. – Showerhead injector, 6-inch combustion chamber, and typical test nozzle.
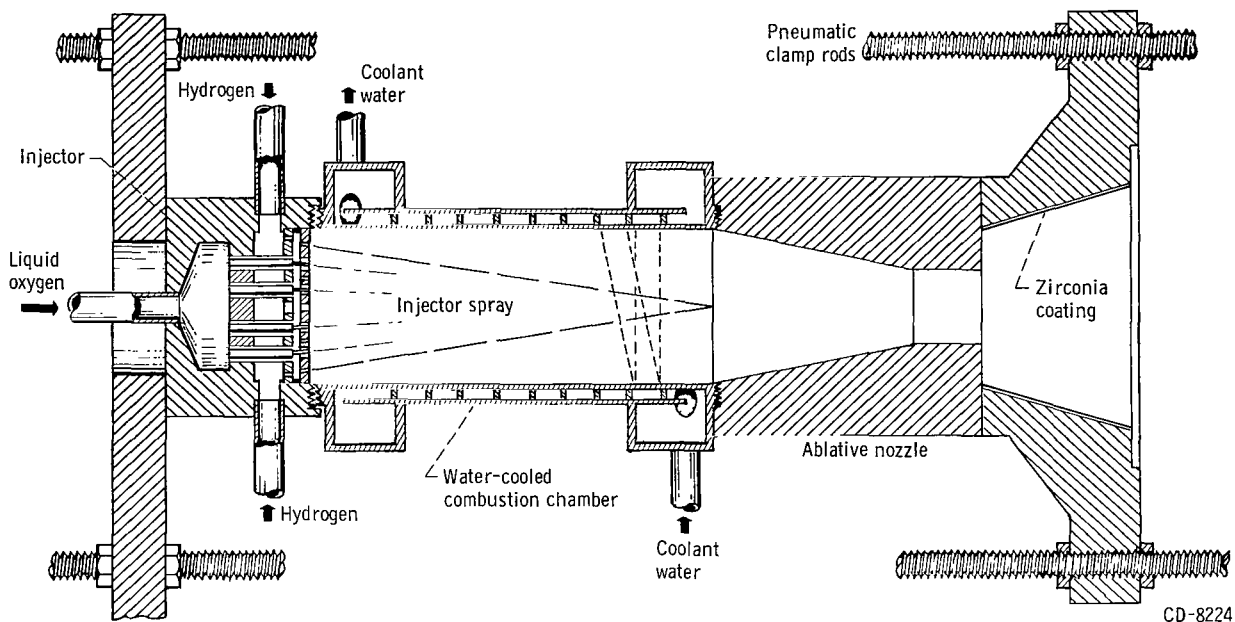
Figure 3. - Schematic drawing of test engine and nozzle.

Injector

Liquid
oxygen

Hydrogen

Coolant
water

Injector spray

Hydrogen

Water-cooled
combustion chamber

Coolant
water

Pneumatic
clamp rods

Zirconia
coating

Ablative nozzle
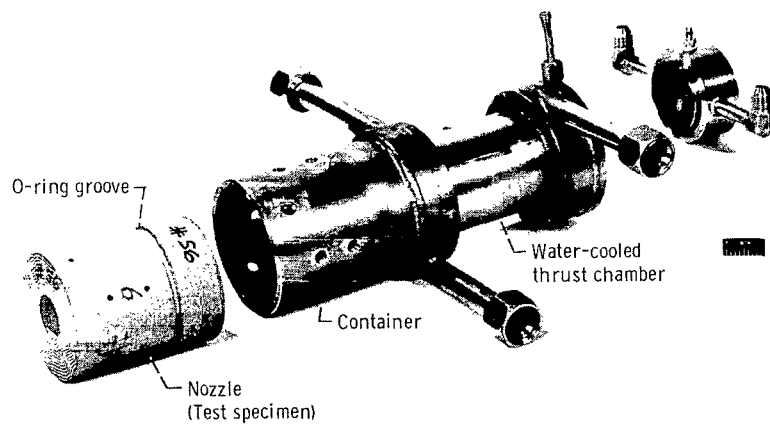
CD-8224

Figure 4. - Ablative nozzle mounting hardware.

O-ring groove

#56

Water-cooled
thrust chamber

Container

Nozzle
(Test specimen)

C-69756

Gas flow

Water-
cooled
thrust
chamber

Metal
O-ring
seal

Test
specimen

Metal
gasket

CD-8228

Figure 5. – Details of noncompressed nozzle mounting.

16

A - A

Liquid
oxygen

Pressure tap   Thermocouple

3/4-in.-long 10 52 NF
stainless steel bolt

Dome

Gasket

A   A

Gaseous   Gaseous
hydrogen   hydrogen

C   C

Injector body   Faceplate   Fuel   Oxidant tubes (12)
                                       distribution
                                       plate

B - B

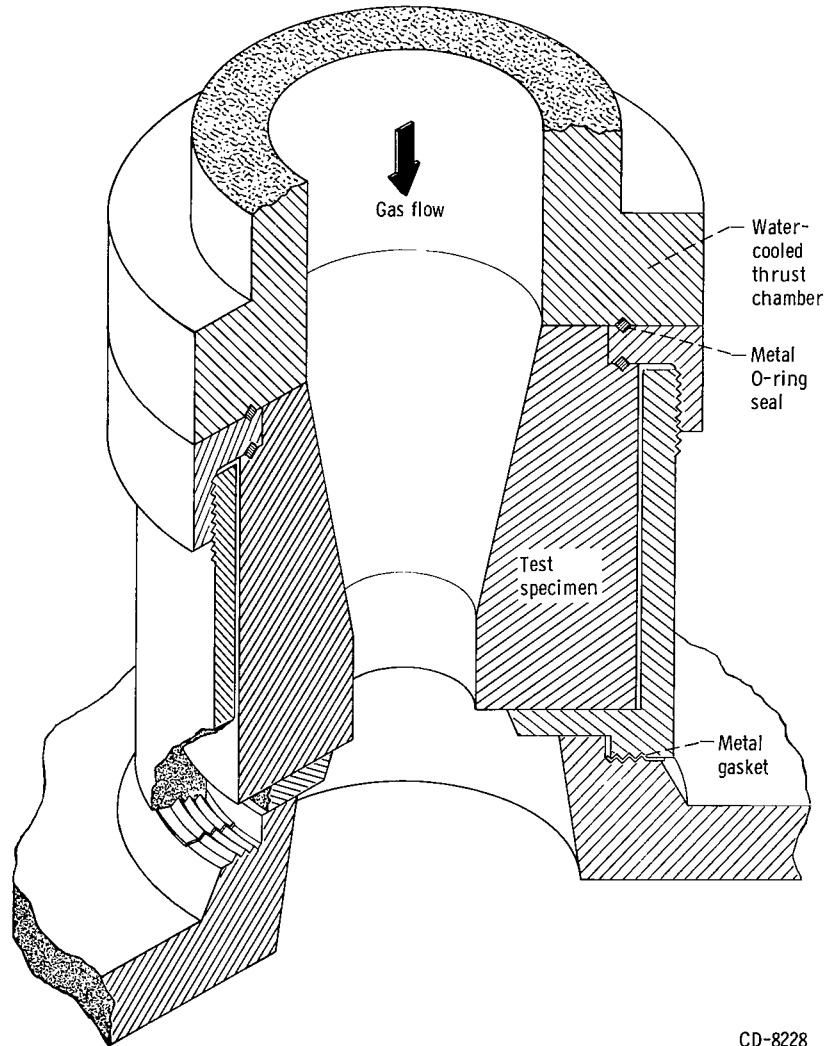Oxygen jets   Hydrogen jets

B   B
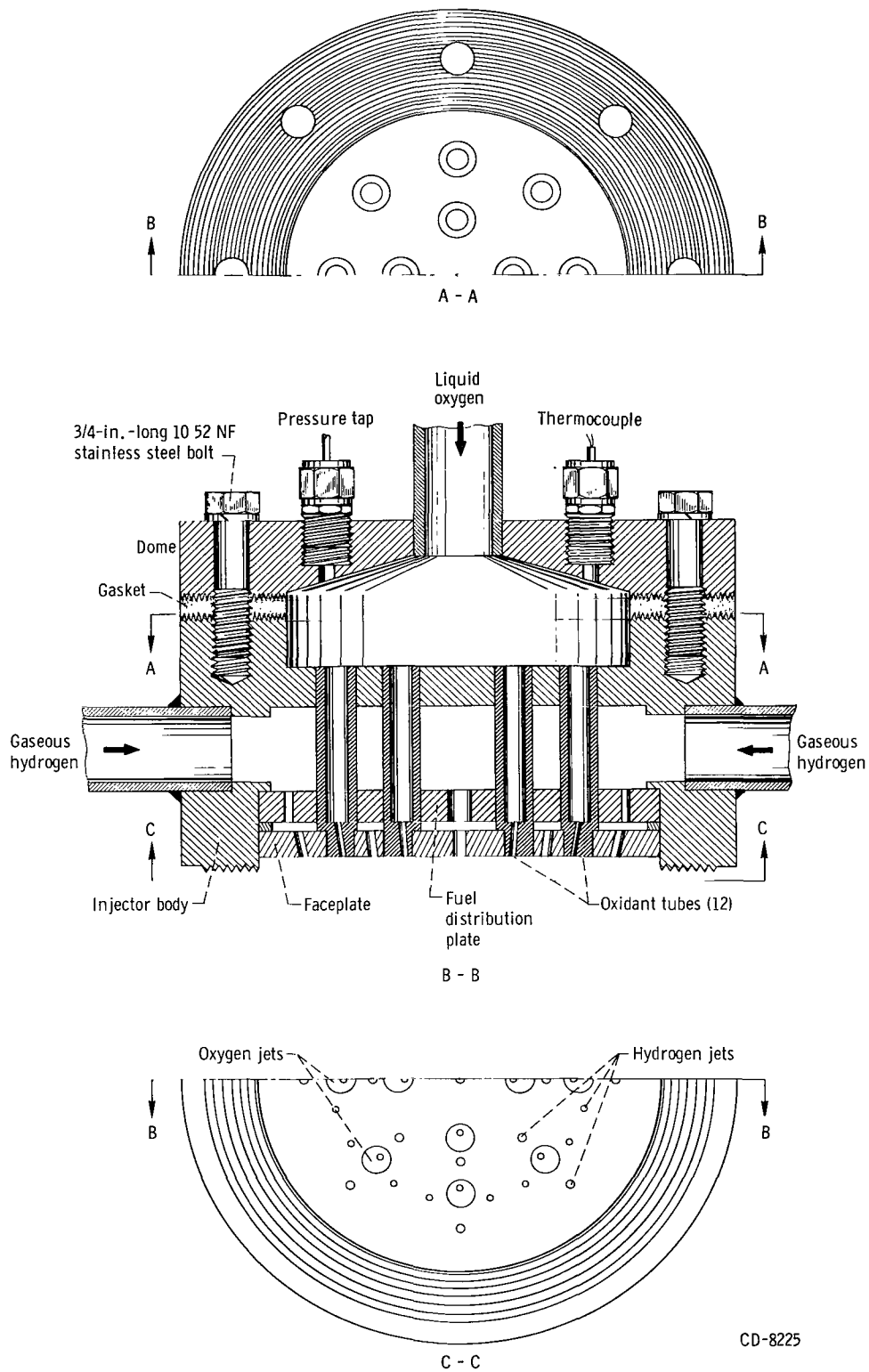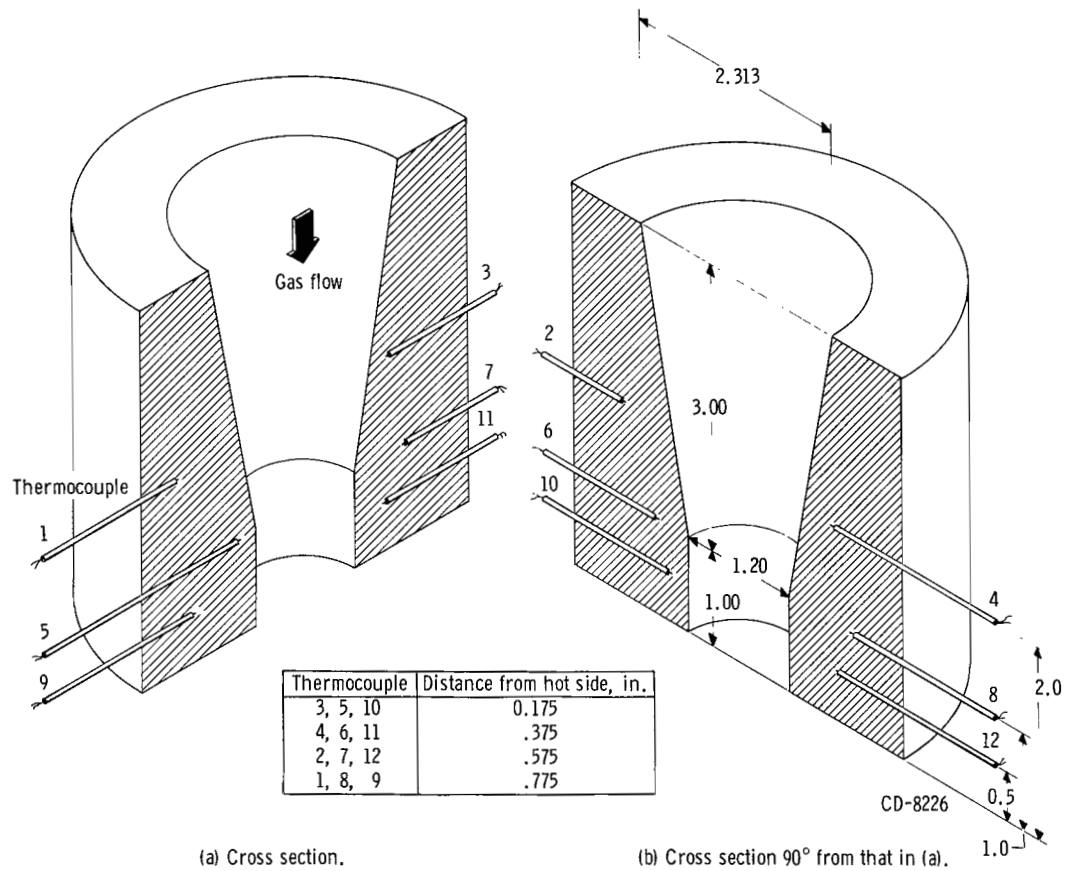
CD-8225

C - C

Figure 6. – Details of converging showerhead injector.

17

(a) Cross section.

(b) Cross section 90° from that in (a).

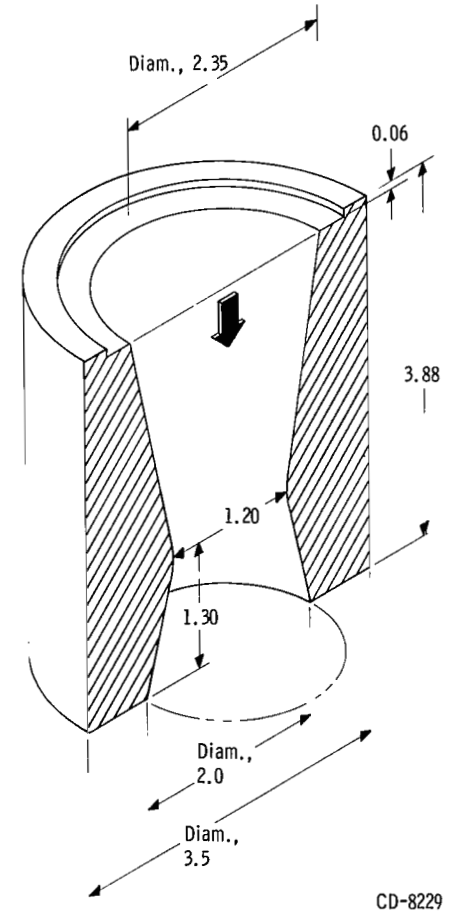Figure 7. – Nozzle detail and thermocouple locations. (Dimensions in inches.)

Thermocouple	Distance from hot side, in.
3, 5, 10	0.175
4, 6, 11	.375
2, 7, 12	.575
1, 8, 9	.775

CD-8226

CD-8229

Figure 8. – Details of contoured heat-sink nozzle. (Dimensions in inches.)

Throat
radius
increase,
in.

Area
increase,
percent

██████	0.03	10
▨▨▨▨	.056	20
▨▨▨▨	.113	40

	Rein-force-ment			Resin				
Nozzle	Nonreinforced	Silica	Nonsilica	Epoxy Novolac	Epoxy Novolac and additive	Phenolic	Phenolic and additive	Other
50			×					×
49	×						×	
64			×	×		×		
51			×	× ×		×		×
41			×	× ×		×		
35			×	× ×				×
36			×	× ×		× ×		
40			×	× ×		× ×		
44		×			×			
22		×	×	×			×	
26		×	×				×	
16		×		× ×				
46		×		× ×				
39			×				×	
23		×		× ×				
19		×		× ×				
45		×			×			
34		×			×		×	
20		×			×			
58			×				×	
59			×				×	
18	×				×			
52		×					×	
38		×						×
47		×				× ×		
37		×				× ×		
48		×					×	
42		×					×	
17		×				×		
53		×						×
30		×					×	
43		×					×	
65		×				×		
29		×					×	
28		×					×	
66		×					×	
55		×					×	
32-3		×					×	
67		×					×	

Nozzle

0   200   400   600   800   1000
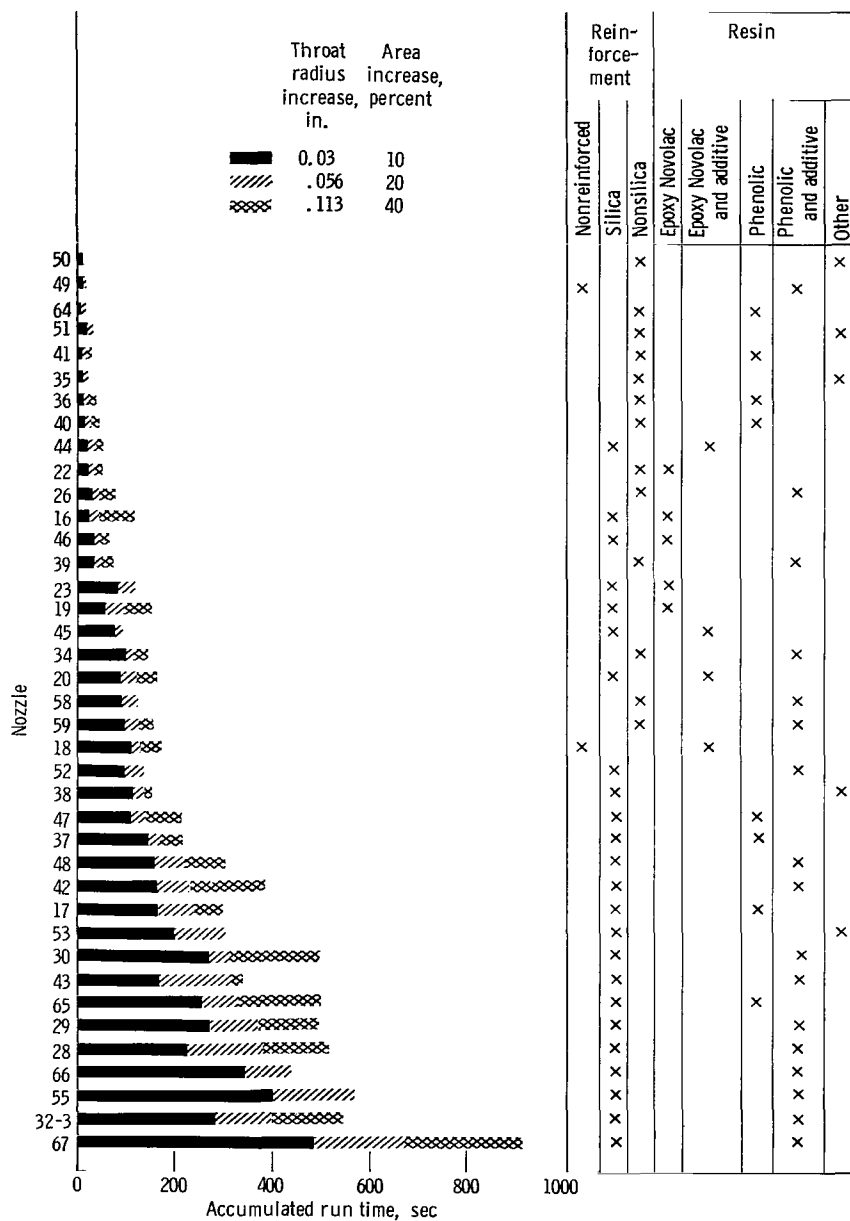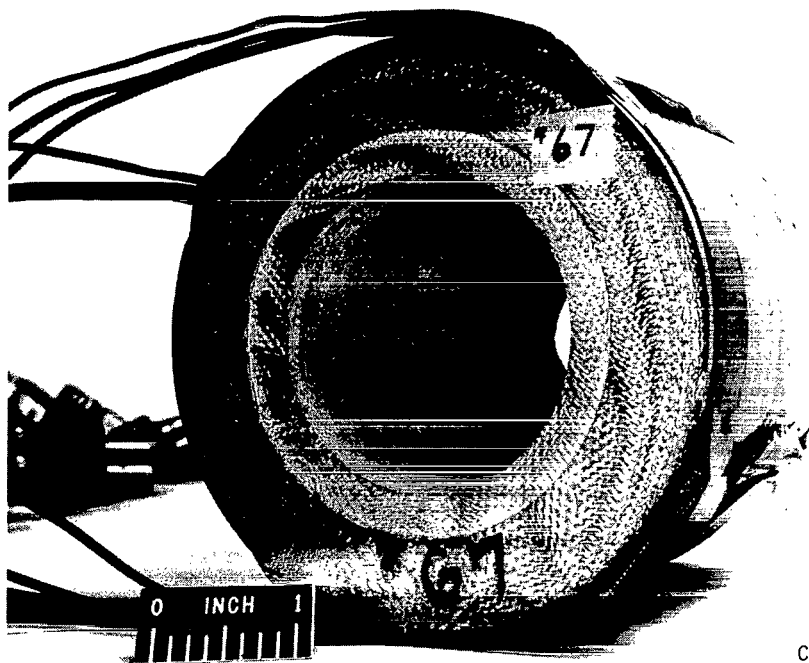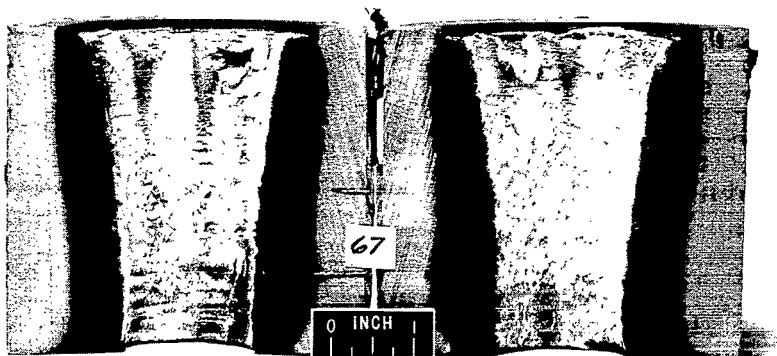Accumulated run time, sec

Figure 9. – Total run duration of ablative nozzles for specified throat radius increases.

19

C-67782

(a) Before testing.

C-70060

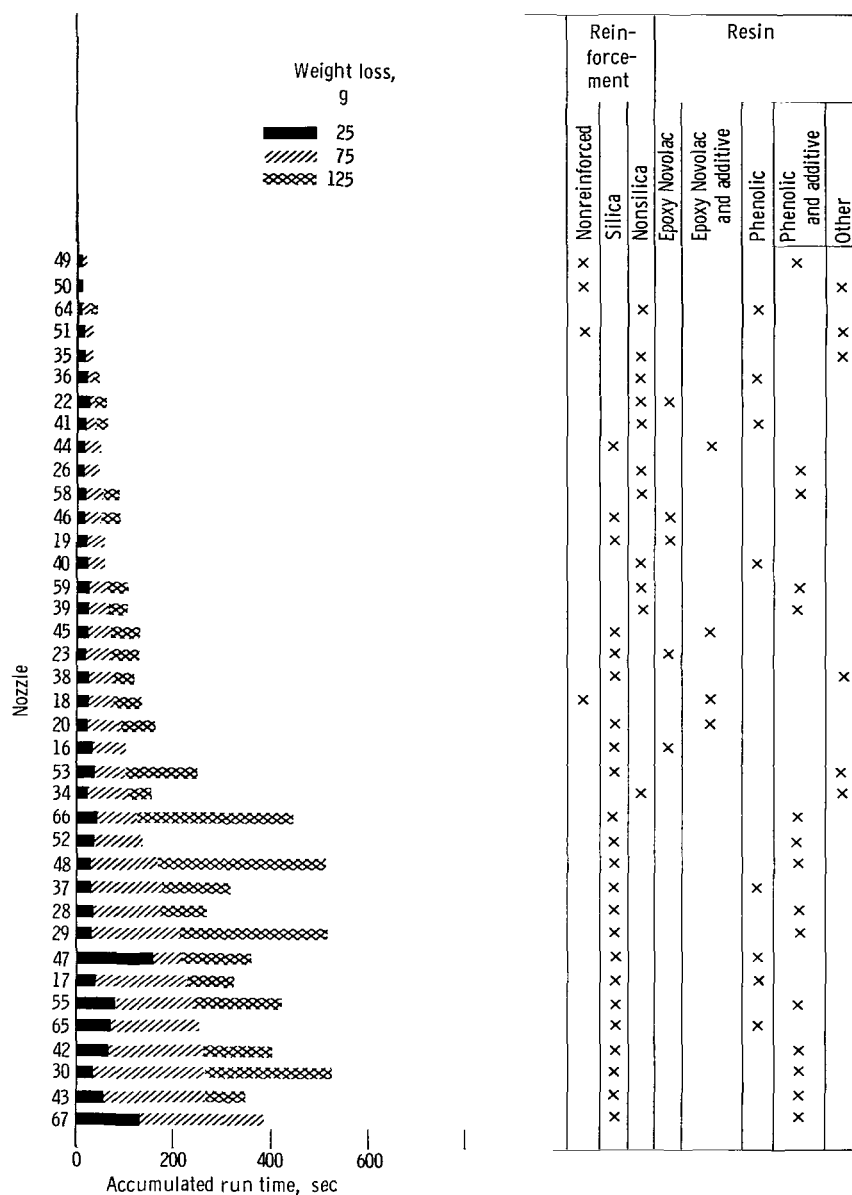(b) After testing.

Figure 10. - Typical test nozzle.

Figure 11. - Total run duration of ablative nozzles for specified weight loss. (Data for 125-g loss not available when not shown.)
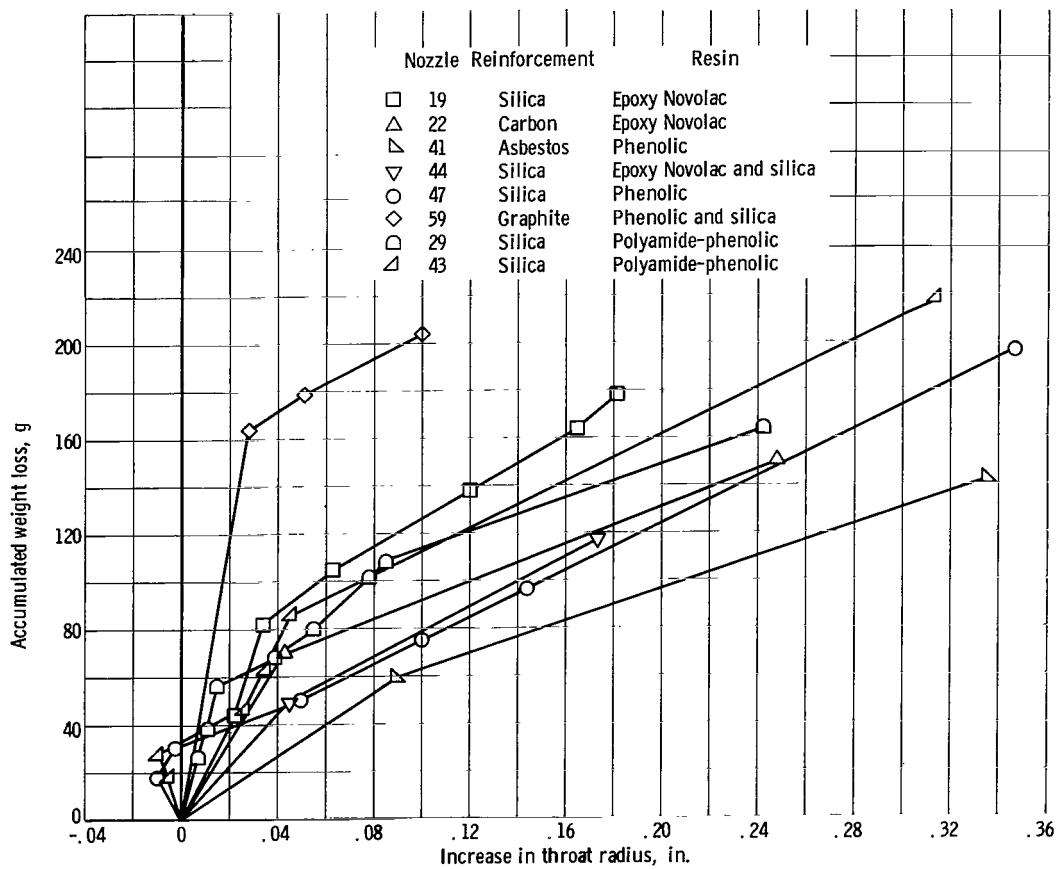
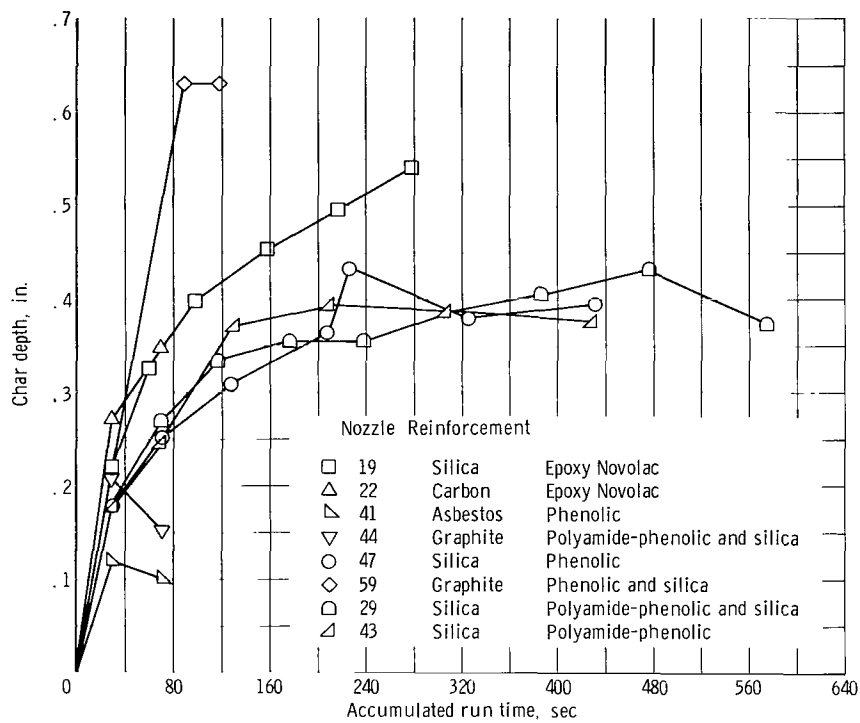Figure 12. – Variation of weight loss with throat radius increase.

Figure 13. - Variation of char depth with run duration (X-ray measurements).
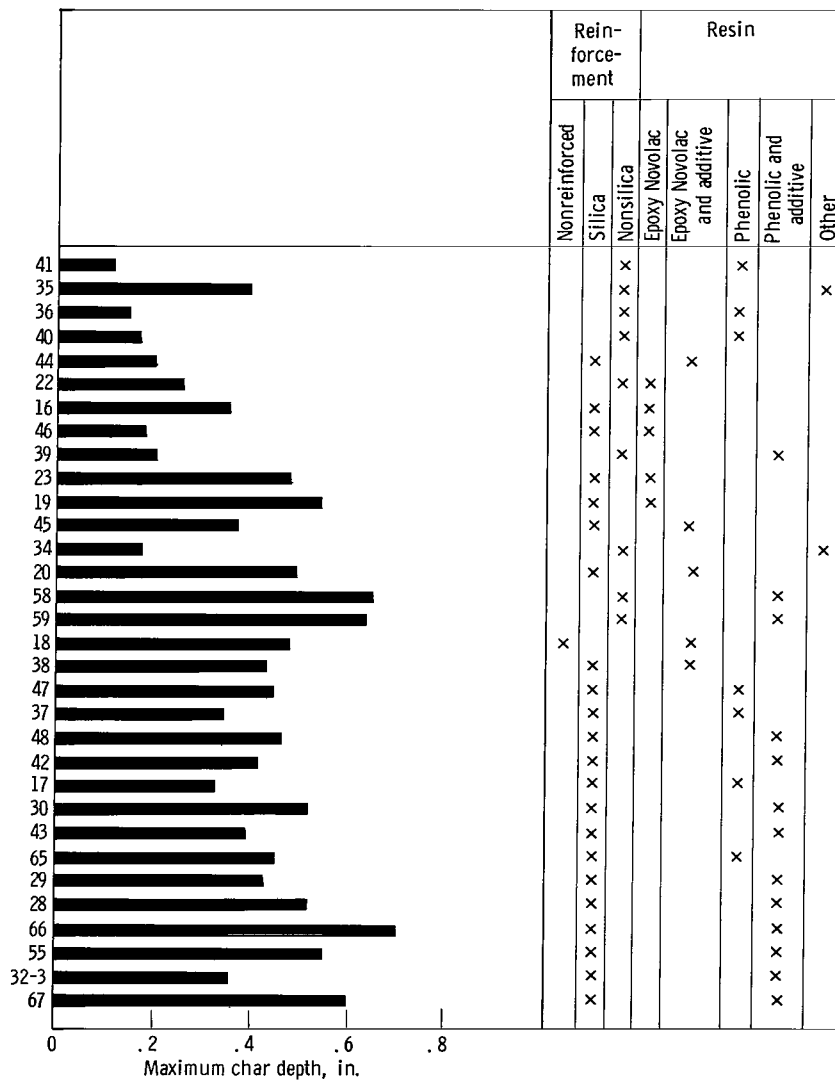
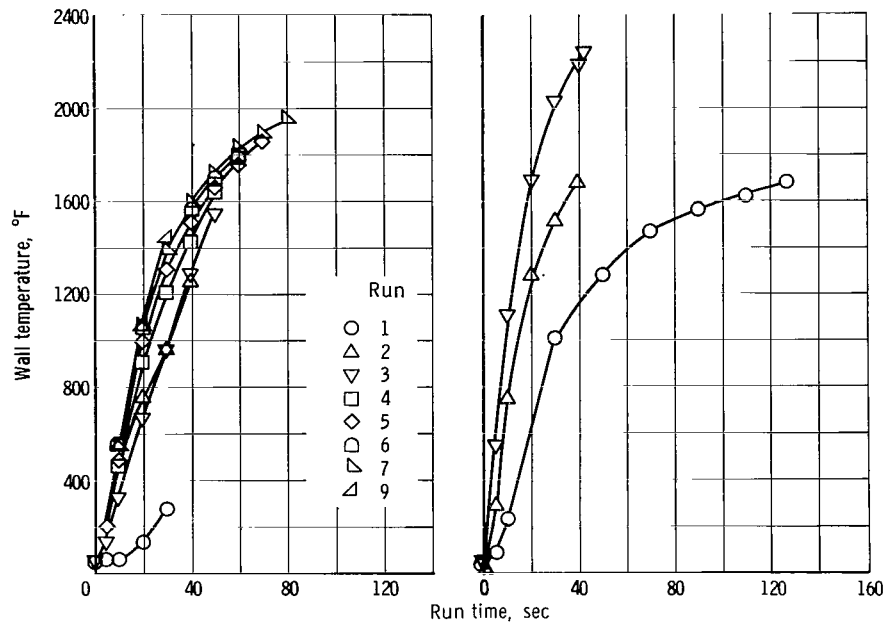The chart shows Char depth, in. (y-axis, 0 to .7) versus Accumulated run time, sec (x-axis, 0 to 640).

Nozzle Reinforcement

	Nozzle		
□	19	Silica	Epoxy Novolac
△	22	Carbon	Epoxy Novolac
◁	41	Asbestos	Phenolic
▽	44	Graphite	Polyamide-phenolic and silica
○	47	Silica	Phenolic
◇	59	Graphite	Phenolic and silica
◠	29	Silica	Polyamide-phenolic and silica
◿	43	Silica	Polyamide-phenolic

23

Figure 14. - Maximum char depth at nozzle throat from X-ray measurement. (Erosion resistance increases from top to bottom of figure.)

	Reinforcement			Resin				
	Nonreinforced	Silica	Nonsilica	Epoxy Novolac	Epoxy Novolac and additive	Phenolic	Phenolic and additive	Other
41			×			×		
35			×					×
36			×			×		
40			×			×		
44		×			×			
22			×	×				
16		×		×				
46		×		×				
39			×				×	
23		×		×				
19		×		×				
45		×			×			
34			×					×
20		×			×			
58		×					×	
59		×					×	
18	×				×			
38		×			×			
47		×				×		
37		×				×		
48		×					×	
42		×					×	
17		×				×		
30		×					×	
43		×					×	
65		×				×		
29		×					×	
28		×					×	
66		×					×	
55		×					×	
32-3		×					×	
67		×					×	

Maximum char depth, in. (0, .2, .4, .6, .8)

24

(a) Nozzle 30; reinforcement, silica cloth.

(b) Nozzle 39; reinforcement, graphite cloth.

Figure 15. – Variation of temperature near throat surface with run duration for consecutive runs.
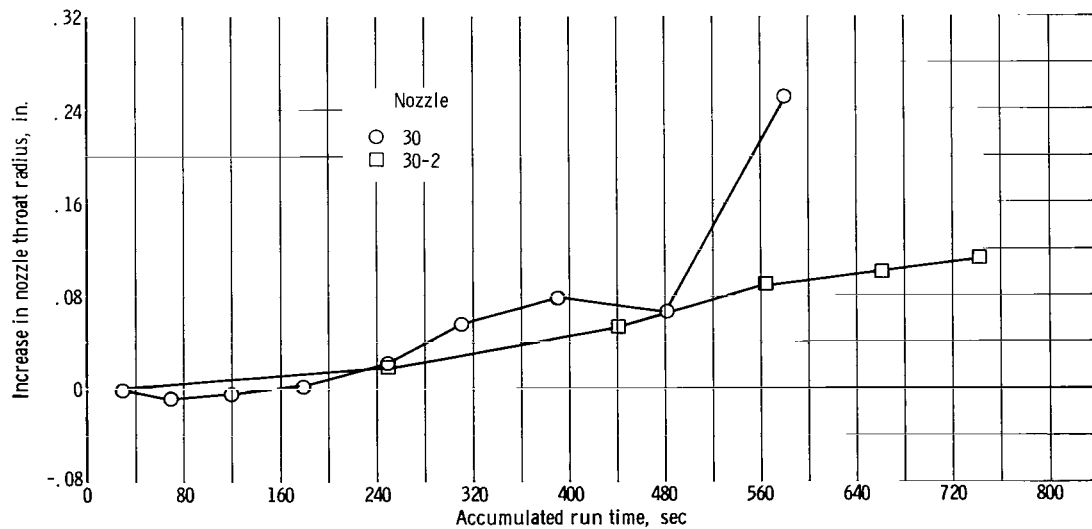

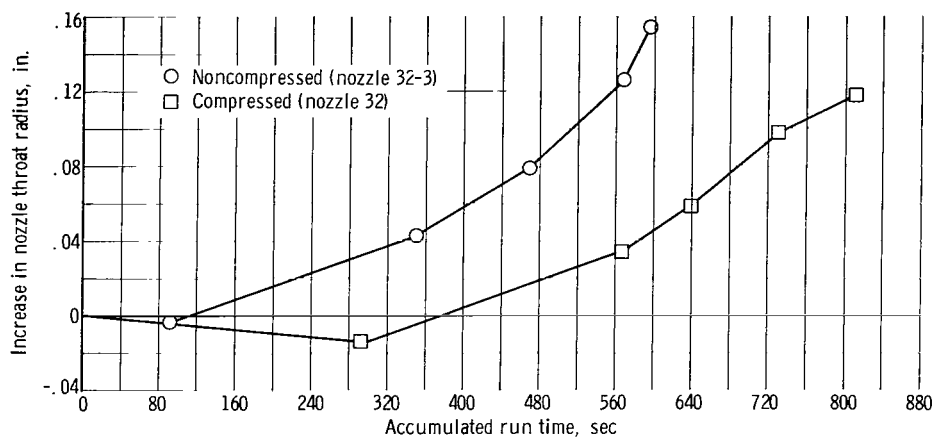Figure 16. – Effect of run duration on nozzle throat erosion rate.

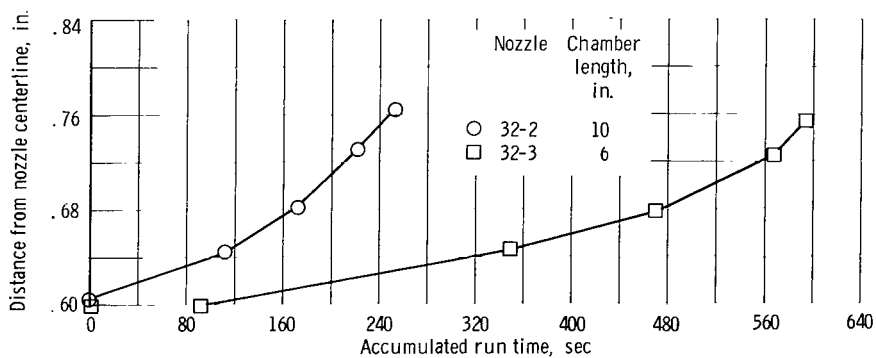Figure 17. – Effect of axial compression of nozzle on nozzle throat erosion rate.

Figure 18. – Effect of combustion chamber length on nozzle throat erosion rate.

NASA SCIENTIFIC AND TECHNICAL PUBLICATIONS

TECHNICAL REPORTS: Scientific and technical information considered important, complete, and a lasting contribution to existing knowledge.

TECHNICAL NOTES: Information less broad in scope but nevertheless of importance as a contribution to existing knowledge.

TECHNICAL MEMORANDUMS: Information receiving limited distribution because of preliminary data, security classification, or other reasons.

CONTRACTOR REPORTS: Technical information generated in connection with a NASA contract or grant and released under NASA auspices.

TECHNICAL TRANSLATIONS: Information published in a foreign language considered to merit NASA distribution in English.

TECHNICAL REPRINTS: Information derived from NASA activities and initially published in the form of journal articles.

SPECIAL PUBLICATIONS: Information derived from or of value to NASA activities but not necessarily reporting the results of individual NASA-programmed scientific efforts. Publications include conference proceedings, monographs, data compilations, handbooks, sourcebooks, and special bibliographies.

Details on the availability of these publications may be obtained from:

SCIENTIFIC AND TECHNICAL INFORMATION DIVISION

NATIONAL AERONAUTICS AND SPACE ADMINISTRATION

Washington, D.C. 20546